Optics & Laser Technology 171 (2024) 110475

Contents lists available at ScienceDirect

Optics and Laser Technology

journal homepage: www.elsevier.com/locate/optlastec

Full length article

Bessel beams as a versatile tool to generate embedded devices in optical glasses☆

Jorge Fantova [a,b], Ainara Rodríguez [a,b,*], Jesús del Hoyo [c], Gemma G. Mandayo [a,b], Santiago M. Olaizola [a,b]

[a] Ceit-Basque Research and Technology Alliance (BRTA), Manuel Lardizabal 15, Donostia/San Sebastián, 20018, Spain
[b] Universidad de Navarra, Tecnun, Manuel Lardizabal 13, Donostia/San Sebastián, 20018, Spain
[c] Grupo Complutense de Óptica Aplicada, Departamento de Óptica, Facultad de Ciencias Físicas, Universidad Complutense de Madrid, Plaza de las Ciencias S.N., Madrid, 28040, Spain

ARTICLE INFO

Keywords:
Ultrafast laser writing
Bessel beams
Nonlinear optical materials
Volume gratings

ABSTRACT

Beam shaping offers many opportunities to both streamline and accelerate laser fabrication processes, closing the gap between lab research and large-scale manufacturing. In the field of embedded devices, a Bessel beam configuration allows for large volume engraving of transparent materials in a single laser pass. In this work, we take advantage of femtosecond Bessel beams with a length of 340 μm and a diameter of 1 μm to generate diffractive elements within three distinct optical glasses. This strategy represents a chemical-free and cost-effective alternative to the conventional manufacturing of holographic elements based on photoresist micro-patterning. Despite the different nonlinear effects taking place in each material, we report the successful fabrication of diffraction gratings operating at either normal or Bragg incidence, with efficiencies in the first combined order of up to 70%. Our experimental results show the potential of Bessel beams as a tool to produce buried light devices in a wide variety of glass materials.

1. Introduction

The interest for diffraction gratings written within transparent materials has been a staple in fields like spectroscopy [1], telecom [2] or astronomy [3], since these photonic devices offer very precise and efficient methods to control light, such as beam multiplexing [2], wavelength filtering [4] or pulse stretching [5], to name a few. The typical route for volume grating (VG) fabrication [6] involves micropatterning of a dichromated gelatin, which is then sandwiched between glass plates [3,7]. Direct laser writing using femtosecond pulses, however, has been proven as a versatile and straightforward alternative due to its ability to generate different types of bulk material structuring [8] in a plethora of dielectrics [9–12].

As ultrashort and intense femtosecond pulses are concentrated within a transparent material, nonlinear light-matter interactions, such as avalanche ionization and multiphoton absorption [13], take place, generating a hot electron plasma in the focal region. When said plasma is relaxed, the energy is transferred to the lattice, which can entail material modifications such as melting, ion migration or the formation of color centers, among other effects [8,14]. Depending on the intensity of the pulse deposition, three distinct regimes of volume engraving can be identified: a smooth isotropic refractive index change (Δn) [15], linked to lower fluence values; birefringent Δn [10], tied to the appearance of nanogratings; and micro-void formation [16], which takes place at higher irradiances. These are typically labeled as type I, type II and type III modifications, respectively [17], and they constitute a permanent structuring of the material.

The diffraction efficiency of engraved VGs heavily depends on the induced Δn and the thickness of the modified region, as both of them determine the phase change generated [18]. The response of each glass to femtosecond laser irradiation varies greatly depending on their composition [9–11], the pulse repetition rate used [19] or the wavelength of the source [20,21], but all in all it is common to induce relatively low Δn, in the range of 10^{-3} to 10^{-2} [9,22]. In contrast, some authors reported Δn values of 0.13 [23] and 0.26 [24] using dichromated gelatins. Therefore, a thicker volume engraving may be necessary to achieve optimal diffraction efficiency. Successive stacking of multiple

☆ This work has been supported by the Ministerio de Ciencia e Innovación (Spain): Retos Colaboración 2019, grant Teluro-AEI (RTC2019-007113-3) and the European Union; and Retos Colaboración 2021, grant BIOFOT (CPP2021-009001). Beam imaging automatization software was developed by Luis Omeñaca, from CEIT-Basque Research and Technology Alliance (BRTA).

* Corresponding author at: Ceit-Basque Research and Technology Alliance (BRTA), Manuel Lardizabal 15, Donostia/San Sebastián, 20018, Spain.
E-mail address: airodriguez@ceit.es (A. Rodríguez).

https://doi.org/10.1016/j.optlastec.2023.110475
Received 7 July 2023; Received in revised form 4 December 2023; Accepted 14 December 2023
Available online 21 December 2023

laser-processed layers is the usual approach to solve this issue [25–27], but due to the limited depth of focus of regular Gaussian beams, which is typically of few microns, this can be very time-consuming [25]. One strategy to overcome this relies on the use of Bessel Beams, which consists in a diffraction-free conical wavefront that interferes along an elongated volume, which is referred to as 'Bessel zone', to generate an intense central lobe of energy. The length of such region can range from hundreds of microns up to meters [28,29] depending on variables such as the wavelength of the beam and the optical system employed. Using such beams, one can achieve both high resolution fabrication and a substantial reduction of processing times, resulting in a simpler, single laser pass engraving of transparent materials [30].

Although the use of ultrafast Bessel beams for the generation of diffractive elements within fused silica has been widely studied [31–33], there are fewer reports exploring this application in other useful dielectrics [30,34,35], let alone works comparing laser-induced volume modifications among different materials using the same writing system. In view of this, this work focuses in the use of long (≈340 μm) Bessel beams to fabricate these devices in three glasses with very different properties: a quantum dot-doped glass (OG530), an alkali-free borosilicate (Eagle2000) and fused silica. Furthermore, by engraving multiple materials with the same 1030 nm source we demonstrate the versatility of the strategy to produce efficient gratings. After the single laser pass processing, the morphology of the inscribed tracks is extensively studied using optical microscopy. Finally, the optical elements are impinged with a HeNe source at different incidence angles to record their diffraction behavior.

2. Materials and methods

2.1. Ultrashort pulse laser processing setup

For the fabrication of the volume gratings we employed an Yb-doped fiber laser source (Satsuma HP, Amplitude) emitting 280 fs, vertically polarized 1030 nm pulses with an output beam diameter of 2.5 mm and a $M^2 < 1.1$. After pulse energy regulation, the Gaussian wavefront was transformed into a Bessel Beam (BB) after incidence onto a 1° off-axis reflective axicon supplied by Cailabs. The beam was then relayed by two consecutive telescopes, resulting in a 10x demagnification factor, to the Bessel zone used for processing, following Fig. 1.a diagram. The 20x microscope objective (MO), with a NA = 0.4 and focal length (f) of 10 mm, provided a writing BB with a conical angle of 20°, a Bessel zone 340 μm long at $1/e^2$ and a central lobe with a FWHM of 1 μm. Its longitudinal propagation profile can be observed in Fig. 1.b. To obtain this plot, the beam was reflected by a mirror placed on the motorized stage and subsequently imaged onto a CCD camara, following the blue-dotted line drawn in Fig. 1.a. Afterwards, over 200 snapshots of the transversal beam profile were taken along the propagation path, which were then combined to generate Fig. 1.b.

Sample scanning was provided via Aerotech ATS100 linear stages. Each track of the grating was fabricated in a single laser pass along the Y axis, as per the coordinate system defined in Fig. 1.a, at a processing speed of V and using a fixed pulse rate of 500 kHz. The tracks were engraved with a periodicity of Λ in the X axis, ultimately producing 3 × 3 mm (X-Y) wide gratings with a varying thickness of L (along the Z axis). The combination of both the high aspect ratio of the BB and the use of large pulse overlaps, e.g. 99.6% when using a V of 2 mm/s, entailed the production of a 'plane' of laser-induced modification for each of the processed tracks. A visual overview of the scanning strategy can be seen in Fig. 1.c. The beam was focused approximately at a depth equal to half the thickness of the correspondent substrate. Table 1 summarizes the range of laser processing conditions used in this work.

2.2. Materials

The research was focused in volume engraving of three dielectrics: a quantum dot-doped borosilicate (OG530), an alkali-free borosilicate (Eagle2000) and UV fused silica, all of which share reports of high refractive index change generation in fs-laser written elements [9,19,36]. In particular, OG530 is a highly nonlinear glass containing 1 vol% of CdS_xSe_{1-x} nanocrystals distributed in its bulk and it is typically sold as a long-pass filter. Eagle2000 is a well-known dielectric for bulk modification, in applications such as low-loss waveguide Bragg gratings [37]. Lastly, fused silica is a robust glass material with an extended commercial use in optics.

All the glass plate substrates were optical-grade two-side polished, displayed a transmittance of over 90% and had a thickness of 1 (Eagle2000 and fused silica) to 2 mm (OG530). A summary of other relevant mechanical and optical properties can be found in Table 2, including the nonlinear refractive index of OG530 [38], Eagle2000 [39] and fused silica [40].

2.3. Volume gratings characterization

Diffraction efficiency measurements were carried out by impinging the gratings using a 633 nm vertically polarized HeNe source. This was carried out at both their Bragg angle and under normal incidence. Fig. 2 depicts the illumination setup for the latter configuration. The drawing also reflects the order of inscription of the tracks of the gratings previously described (♯1, ♯2...). The intensity of the resulting orders (m) was measured with a power meter (PM) while considering the inherent transmission losses of the glass.

Optical microscopy was used for morphological characterization of the resulting VGs, focusing in the cross-section imaging, i.e. side view, of the devices. For this, the samples were sliced transversal to the sample scanning direction, i.e. at the X-Z plane represented by the green-dotted line in Fig. 2, using a high precision cutting machine (MicroAce Series 3). Then they were observed under the microscope using the bright field transmission mode, illuminating the samples in the Y axis. This allowed for the inspection of the laser-induced tracks generated along the beam propagation axis (Z). Immersion oil was applied to the sliced side of the samples to fill the gaps between the substrate and the sample holder, thus minimizing refractive index mismatch at the interface.

Additionally, the influence of input polarization was studied by inserting a half-wave plate at the output of the source. After such modulation of the azimuth angle of the incident light, the shifts in intensity for each of the diffracted orders were recorded by the PM.

3. Results and discussion

3.1. Laser-matter interactions

When irradiating the samples in the range of experimental conditions shown in Table 1, each material showed quite a different response, as can be seen in Fig. 3. The engraving of OG530 yielded gratings with subtler contrasts, Eagle2000 typically showed alternating bright and dark regions along the propagation length of the pulse, and the modification of fused silica resulted in dark-colored tracks. The following sections examine the characteristic laser-matter interactions registered for each glass after an extensive morphological analysis.

3.1.1. OG530 modification

The elongation of the laser tracks stands out in the case of OG530, which can be clearly seen in Fig. 4, where tracks up to ≈1 mm in length were recorded, far beyond the length of the Bessel zone.

This did not occur to such an extent in the other materials, which could be explained by OG530 having a much larger nonlinear refractive index ($-5.92 \cdot 10^{-18}$ m^2/W, [38]) than Eagle2000 ($3.60 \cdot 10^{-20}$ m^2/W,

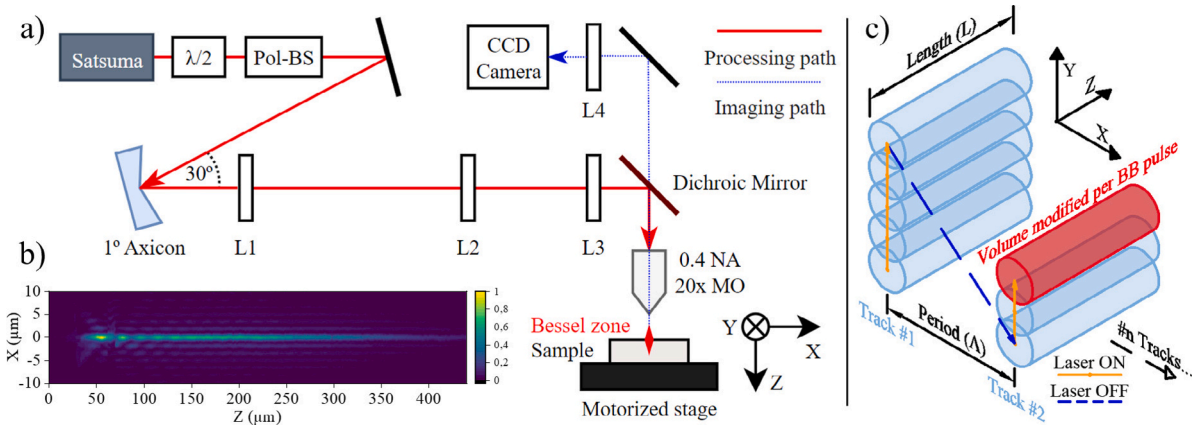

Fig. 1. (a) Sketch of the processing and imaging setup: $f_{L1} = f_{L2} = 250$ mm; $f_{L3} = 100$ mm; $f_{L4} = 400$ mm; $f_{MO} = 10$ mm. (b) Inset of the longitudinal intensity profile of the Bessel Beam, recorded by the CCD camera. (c) Diagram representing the scanning strategy of the laser-processed tracks of the gratings.

Table 1
Range of experimental conditions selected for grating fabrication.

Pulse energy (E_p) [μJ]	Repetition rate [kHz]	Grating period (Λ) [μm]	Processing speed (V) [mm/s]
3.0–12.5	500	5–50	1–8

Table 2
Compendium of properties of the glass substrates.

Material	OG530	Eagle2000	Fused silica
Linear refractive index, n_0 (@633 nm)	1.51	1.50	1.46
Nonlinear refractive index, n_2 [m^2 W^{-1}]	$-5.92 \cdot 10^{-18}$	$3.60 \cdot 10^{-20}$	$2.19 \cdot 10^{-20}$
Thermal expansion coefficient, α (20 °C/300 °C) [10^{-6} K^{-1}]	9.00	3.18	0.54
Transition temperature, T_g [°C]	508	≈717	1480
Softening temperature [°C]	–	985	≈1700

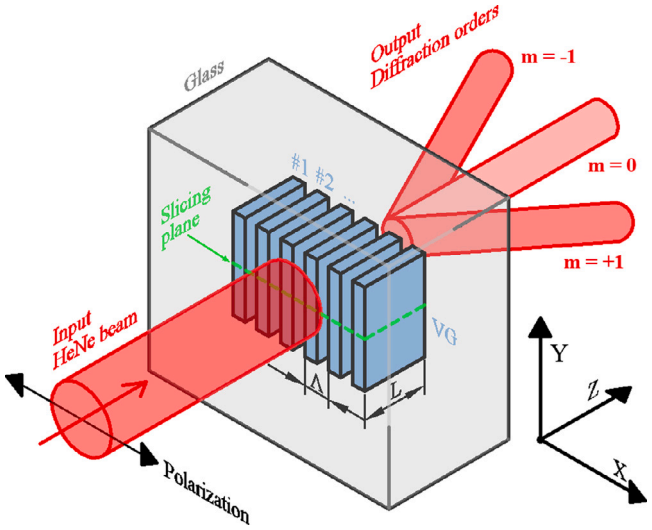

Fig. 2. Diagram of the setup used for the measurement of the diffraction behavior of the fabricated volume gratings. The drawing corresponds to illumination under normal incidence. The coordinate system matches that of Fig. 1. The green-dotted line represents the plane at which the samples were sliced to enable cross-section imaging.

[39]) and fused silica ($2.19 \cdot 10^{-20}$ m^2/W, [40]). A higher nonlinear refractive index promotes Kerr self-focusing effects, as it lowers the energy threshold at which the beam collapses, which is known as critical power (P_{cr}) [13]. This is reflected in the equation defining P_{cr}: $P_{cr} = 3.77\lambda_0^2/8\pi n_0 n_2$ [41]. Here, λ_0 represents the wavelength of the laser beam and n_0 and n_2 the linear and nonlinear refractive index of the material, respectively. When the peak power of the pulse overcomes this threshold, filamentation effects may ensue [13].

The calculated P_{cr} at 1030 nm for OG530, Eagle2000 and fused silica were, respectively: 0.02, 2.93 and 5.01 MW. Considering our source, the emission of a 4 μJ pulse with a duration of 280 fs results in a peak power of 14.29 MW, which is almost 800 times the P_{cr} of OG530 and threefold that of fused silica. These calculations, thus, support the more pronounced filamentation registered for OG530. Such increased nonlinearity, however, is not necessarily a drawback, as Martinez-Vazquez et al. [9] took advantage of this feature to obtain a Δn shift as high as 0.018, making OG530 suitable for the fabrication of efficient volume diffraction gratings.

Aside from the filamentation, the tracks engraved within OG530 were enveloped by a dark cladding, as seen in Fig. 4. This was likely caused by an accumulation of heat within the bulk of the glass, as intra-volume fs pulse irradiation at frequencies over 200 kHz is well-known to overcome heat diffusion rate [22], resulting in temperature buildup and the appearance of volume engraving in regions beyond the length of the Bessel zone. The phenomenon was further enhanced as E_p increased, reaching the point of track overlap despite the 50 μm periodicity, as is shown in Fig. 5. Conversely, when using pulse energies of 4 μJ or lower, a more subtle modification takes place and thinner laser induced-tracks are produced, which can be seen in Fig. 3. Here, the visible bright and dark areas might be attributed to slight positive and negative Δn, respectively [37,42].

3.1.2. Eagle2000 modification

Direct laser writing of Eagle2000 resulted tracks containing alternating bright and dark regions, as in Fig. 3, for most of the engravings performed. Fernandez et al. elaborated in [11] that this clear contrast is owed to the migration of elements (such as Ca, Si or Al) contained in the glass matrix, which produced variations of Δn in the bulk of the material. Furthermore, they analyzed how a modulation of laser

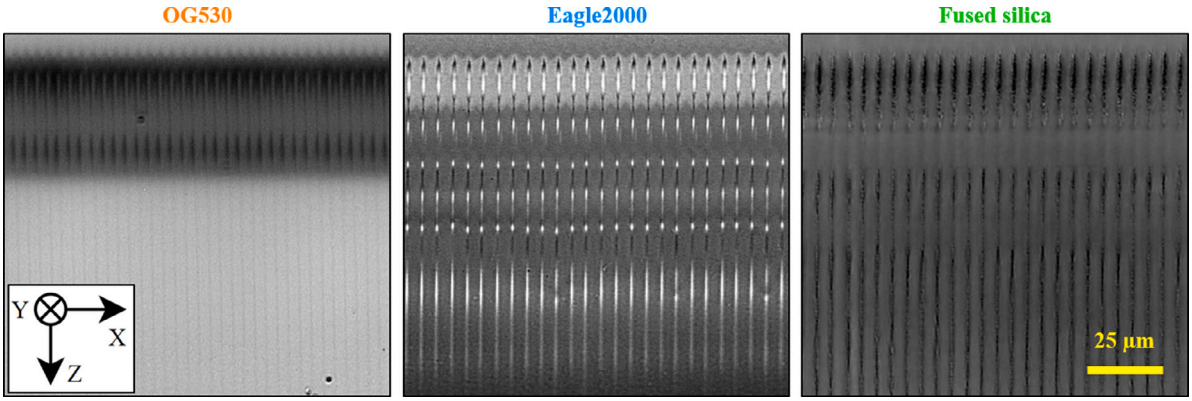

Fig. 3. Transversal optical imaging of the volume gratings inscribed with a period of 5 µm while using a pulse energy of 4 µJ and a processing speed of 4 mm/s. Beam incident from the top. The scale bar applies to all the pictures.

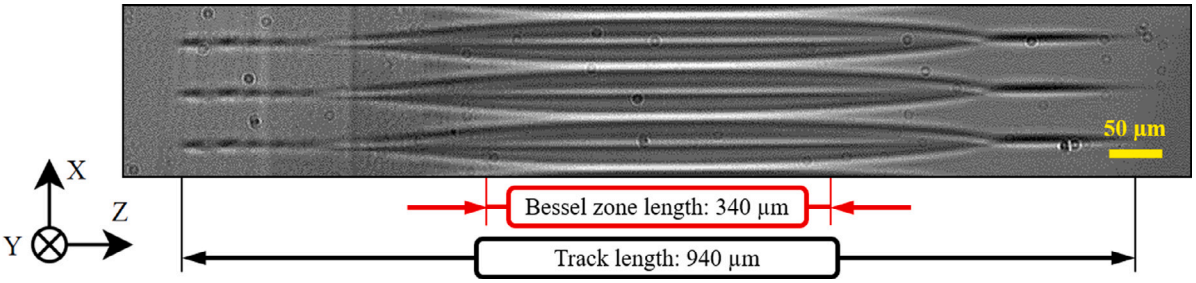

Fig. 4. Comparison between the length of the Bessel zone and the laser-induced modification of OG530 when using a pulse energy of 7.5 µJ and a processing speed of 2 mm/s. Beam incident from the left.

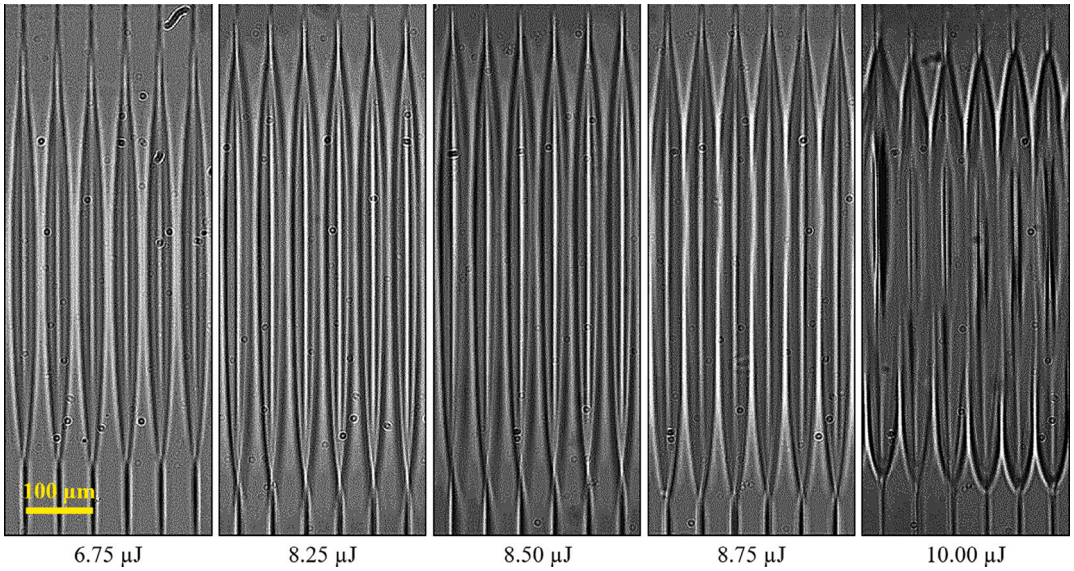

Fig. 5. Cross section of OG530 volume gratings fabricated at different pulse energies with a periodicity of 50 µm and a V of 2 mm/s. The orientation of the images matches that of Fig. 3.

fluence can generate shifts in the sign of the refractive index change, i.e. from positive to negative or vice versa, within the engraved region. For instance, they inverted the value of Δn within the core, i.e. the central region, of Eagle2000 waveguides as fluence was decreased: from $-8 \cdot 10^{-3}$ to $+8 \cdot 10^{-3}$ [11]. In our case, it is worth noting that the pattern at which the bright and dark regions alternate along a single track resembles that of the longitudinal profile of the BB, portrayed in the inset of Fig. 1.b. The oscillation of the energy throughout the Bessel zone, especially at the beginning of the beam [43–45], results in a variation of the effective fluence, which could entail that the bright and dark regions observed in the samples correspond to the alternating shifts between positive and negative Δn described in the literature.

In the case of Eagle2000, heat accumulation started to appear when selecting a pulse energy of 4 µJ or higher. The gray-colored cladding that envelops the beginning of the track in Fig. 3 is a reported symptom of such phenomenon [11,19] and precisely concurs with the point of highest intensity throughout the BB. An increase of E_p led to further enlargement of the tracks, as a shift between 5.25 and 6.75 µJ led to lengths from 325 to 375 µm, respectively, as Fig. 6 portrays. These values are in the order magnitude of the Bessel zone length (340

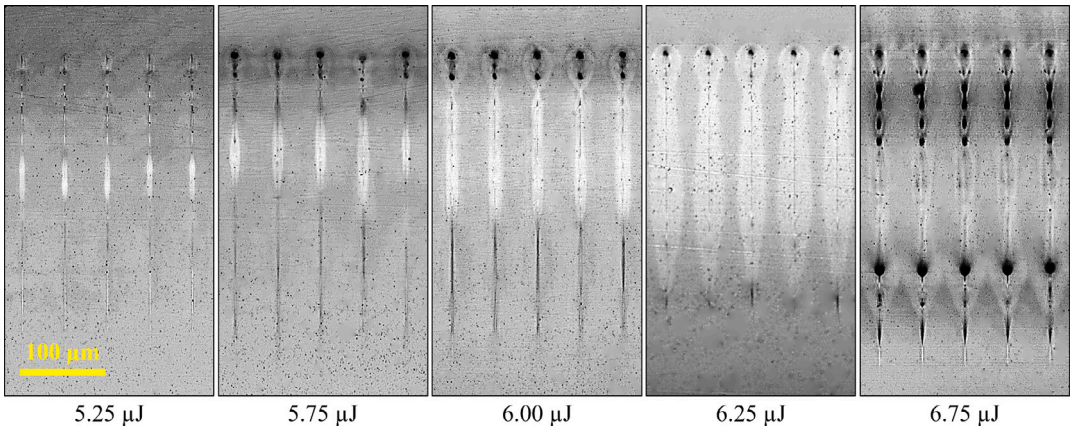

Fig. 6. Cross section of Eagle2000 volume gratings fabricated at different pulse energies with a periodicity of 50 µm and a V of 4 mm/s. The orientation of the images matches that of Fig. 3.

µm) and clearly contrast with the near 1 mm long tracks registered for OG530 (Fig. 4), which means that filamentation effects are less prominent for Eagle2000. This difference in laser-matter interaction is, thus, found in accordance with the aforementioned P_{cr} thresholds of each material.

3.1.3. Fused silica modification

The majority of the examined fused silica gratings, processed with pulses up to 12.5 µJ, showed dark-colored tracks on the optical microscope such as the ones seen in Fig. 3, whose appearance has been linked to the formation of nanogratings in the literature [27]. This contrasts with the OG530 and Eagle2000 tracks (Figs. 5 and 6), where we appreciated the bright and dark regions that are usually associated with positive and negative Δn, respectively [8,36,42]. Because of this, we believe that the laser-induced modifications produced in fused silica will alter the amplitude of incident light to a greater extent than its phase.

When fabricating fused silica gratings with a pitch of 20 µm or lower, a kind of '*shielding*' effect was observed, by which the length of the tracks decreased after the engraving of the first few tracks. In Fig. 7.a–c one can see how the tracks of the 10 and 20 µm period gratings become steadily shorter within the first 3 to 5 lines, after which their size (L) becomes constant. In contrast, this phenomenon did not occur for the 50 µm grating. Since the phenomenon is promoted as track periodicity decreases, this suggests that it is caused by an interaction between the incident Bessel beam and the already-processed tracks, following either absorption or scattering mechanisms, or a combination of both.

When a BB encounters an obstruction in its path, its self-healing properties allow for its reconstruction after a certain propagation distance, whose length is tied to the size of said obstacle in all dimensions and the conical angle of the Bessel beam [46,47]. In spite of this, a partial cropping or disruption of the BB entails a decrease in the intensity of the central lobe of the beam and, consequently, the reduction of the length of the Bessel zone. Because of this, the region within the focal volume whose intensity surpasses the engraving energy threshold will be smaller, hence the decrease of length of the laser-induced tracks.

As for the source of the obstruction in our samples, it could be that, when the BB is being focused in fused silica, the wavefront becomes effectively cropped by the pre-existing neighboring tracks due to their proximity. This would lead to the shortening of the Bessel region and, thus, the length of the inscribed tracks [46] that we acknowledged in Fig. 7. This 'shielding' effect was not registered in neither OG530 nor Eagle2000, even when fabricating 5 µm spaced gratings. We believe that one possible cause for this disparity lies in the aforementioned higher amplitude modulation of incoming light of the fused silica tracks. We see a symptom of this in Fig. 7.d, where the 10 µJ pulses seemingly induced residual stress in the form of ripples in the volume surrounding the tracks. This effect may also occur for lower pulse energies, but it may not be apparent due to image resolution. We hypothesize that this could represent a partial obstruction in the propagation of the BB [47], resulting in additional 'shielding'.

It is worth noting that this phenomenon has not been reported, to the best of our knowledge, in other works using BB to produce embedded gratings in a dielectric. This might be caused by the, comparatively, large focal volume of our BB, as the operating wavelength was 1030 nm and the beam was focused by a factor of 10. The common combination of shorter wavelengths and high demagnification factors selected by most authors [31,48] results in a tighter Bessel zone, which may avoid the interaction of the wavefront with the surrounding tracks and therefore the acknowledged 'shielding' effect.

Lastly, the rise of pulse energy in the case of fused silica only led to the elongation of the tracks, as seen in Fig. 7.(c–d). This contrasts with what both OG530 (Fig. 5) and Eagle2000 (Fig. 6) experienced, where the width of the tracks visibly increased due to the effect of heat accumulation. This phenomenon could be explained by the lower thermal expansion coefficient and higher transition temperature of fused silica, which are displayed in Table 2. Since fused silica is more rigid and requires more temperature to melt than the other glasses, the widening of the tracks in fused silica is less pronounced. Instead, the energy tied to the higher pulse energies seemed to induce residual stress, as can be observed in the middle region of Fig. 7.d, which was processed using 10 µJ pulses.

3.2. Diffraction behavior of the samples

Following the Rigorous Coupled Wave (RCW) theory [49], a diffraction grating can be classified as either a *thin* (or Raman-Nath) grating or a *thick* (or Bragg) grating. In a thin grating the light is, ideally, diffracted evenly between the positive and negative orders under normal incidence, whereas in a thick grating the light is concentrated into a particular diffraction order when incidence is performed at the so-called Bragg angle. This differentiation depends on the value of the so-called thickness parameter Q [50]: a $Q < 1$ promotes the thin regime, while a value of Q around 10 and above facilitates the thick regime behavior. This parameter is defined in Eq. (1), where λ is the illumination wavelength, L is the thickness of the grating and n is the average refractive index of the medium.

$$Q = \frac{2\pi\lambda L}{n\Lambda^2} \tag{1}$$

The gratings fabricated with $\Lambda > 20$ µm yielded Q values close to 1 and were consequently illuminated under normal incidence, while those with a period of 5 µm showed a Q over 50, thus belonging

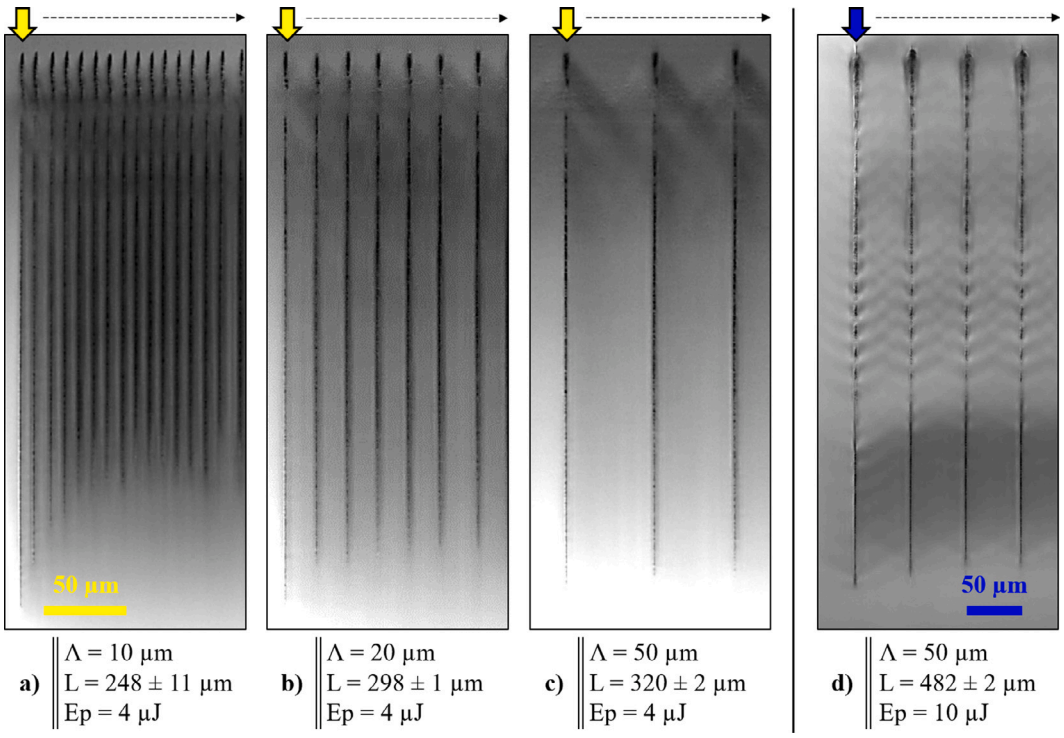

Fig. 7. Cross-section of fused silica volume gratings engraved at different periods (Λ) and pulse energies (Ep) with a fixed processing speed (V) of 4 mm/s, yielding different track lengths (L). The tracks were inscribed from left to right, starting from the one indicated by the colored arrow (i.e. 'Track ♯1' as depicted in both Figs. 1.d and 2). The yellow scale bar applies to (a), (b) and (c). The orientation of the images matches that of Fig. 3.

Table 3
Summary of the conditions of the highest performing diffraction gratings for both illumination conditions.

Material	Normal incidence					Bragg angle incidence				
	Ep [µJ]	Λ [µm]	Q	$\eta_{m\pm1}$ [%]	η_{Total} [%]	Ep [µJ]	Λ [µm]	Q	$\eta_{m\pm1}$ [%]	η_{Total} [%]
OG530	8.5	50.0	1.36	41.8	90.2	4.0	5.0	89.70	67.5	88.3
Eagle2000	6.0	35.0	1.49	70.6	81.9	3.5	5.0	58.50	54.8	92.1
Fused Silica	4.0	20.0	3.78	14.2	85.8	3.5	5.0	50.77	65.1	88.2

to the thick regime. Considering this, they were each impinged with the HeNe source at the appropriate angle of incidence for maximum diffraction efficiency. Table 3 summarizes the best results obtained for both illumination conditions and the three materials, along with the period of the resulting gratings, their Q and the E_p used in their fabrication. Building on these data, the upcoming sections explore further the diffraction behavior of both sets of gratings.

3.2.1. Normal incidence

In order to promote thin-grating performance, 50 µm pitched elements were recorded with a processing speed (V) of 2 mm/s at different pulse energies, registering their diffraction behavior in Fig. 8 for each material. Peak efficiencies for the combined first order were recorded for both OG530 (41.8%) and Eagle2000 (59.7%), while fused silica did not show this tendency. These maxima can be enhanced by tuning parameters such as Λ or V, as choosing a $\Lambda = 35$ µm, a $V = 4$ mm/s and 6 µJ pulses yielded a VG with an efficiency of 70.6% in Eagle2000. After collecting these results, the cross-section of the samples surrounding the respective diffraction peaks for both OG530 (Fig. 5) and Eagle2000 (Fig. 6) was examined.

According to the RCW theory, the diffraction efficiency of the m_{th} order for a thin binary phase grating follows a sinusoidal trend, as expressed by Eq. (2) [51], where $\Delta\varphi$ represents the phase accumulation generated. As can be drawn from the definition of this variable in Eq. (3), the diffraction efficiency is ultimately dependent on L and Δn.

$$\eta_m = sinc^2\left(\frac{m\pi}{2}\right) cos^2\left[\frac{1}{2}(\Delta\varphi - m\pi)\right] \tag{2}$$

$$\Delta\varphi(x) = \frac{2\pi}{\lambda} L \cdot \Delta n(x) \tag{3}$$

For OG530 and Eagle2000, each group of the gratings presented in Fig. 8 had similar L, respectively. Even though the shape of the tracks was not homogeneous, bright regions resembling an isotropic phase change, i.e. type-I modification [8], were apparent within their core, which entails that the effective Δn induced at a certain pulse energy resulted in a peak value in the sinusoidal function, concurring with the diffraction peaks shown in the graphs of Fig. 8.

The absence on this maximum in fused silica gratings could be linked to their low effective duty factor, as we see in Fig. 7.c–d that the width of the tracks remained essentially unchanged regardless of the Ep used, reaching a value of ≈3 µm after the engraving with 10 µJ pulses. This accounts for a duty factor of 6%, which is far from the 50% that promotes the diffraction of phase gratings in the first combined order [52]. In contrast, we saw in Figs. 5 and 6 that the increase of Ep led to the widening of the tracks in both OG530 and Eagle2000, respectively, due to heat accumulation. This could be providing the gratings with an effective duty factor closer to 50%, as the cladding that envelops the tracks also entails a refractive index change over the medium [11], which would explain the peak diffraction performance of the 50 µm period gratings in OG530 and Eagle2000 shown in Fig. 8.

3.2.2. Bragg angle incidence

To generate Bragg gratings, 5 µm pitched elements were engraved on all dielectrics at a pulse energy of 3.5 to 4.0 µJ while varying V.

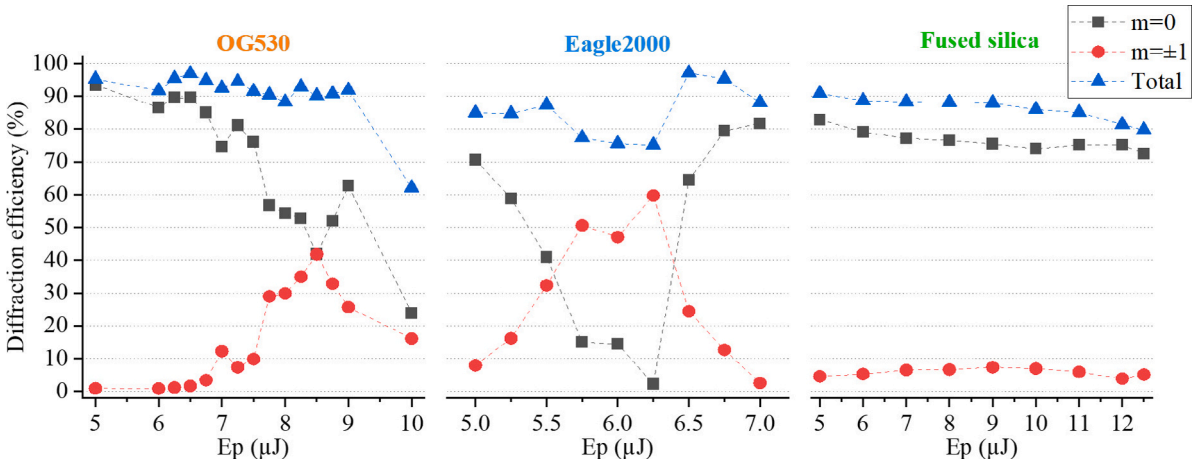

Fig. 8. Influence of pulse energy on the diffraction efficiency at different orders, while under normal incidence, for OG530, Eagle2000 and fused silica volume gratings, all fabricated with a period of 50 μm.

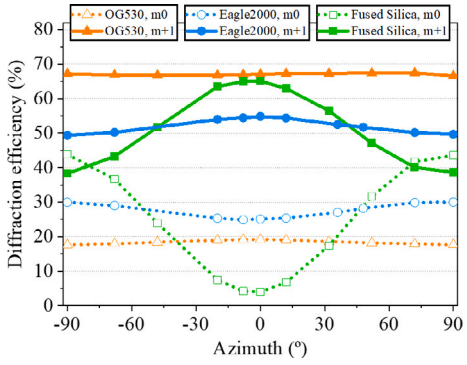

Fig. 9. Diffraction efficiency of the volume gratings of Fig. 3 after illumination at different polarization states. Incidence at the Bragg angle condition.

Their diffraction performance was measured at Bragg angle incidence, yielding the highest efficiencies in the first order when using 4.0 μJ pulses and a V of 4 mm/s: ≈65% for OG530 and fused silica and almost 55% for Eagle2000. Total transmittance for all samples was above 85%. We show the cross-section of these gratings in Fig. 3.

The samples were then impinged at different beam polarizations while maintaining Bragg angle incidence. In Fig. 9 one can see how the change from vertical (±90°) to horizontal polarization (0°) influenced mainly fused silica, attenuating the zeroth order by 90% and enhancing the first order by 70%. The gratings inscribed in the other glasses, however, were almost unaffected by this shift in the azimuth angle. These results are in line with those of Beresna et al. in [53], where relative intensity between the diffraction orders was modified as the input polarization changed due to the effect of nanogratings. Thus, this suggests their presence in, at least, the studied sample.

4. Conclusions

In this work, we have shown the versatility of ultrashort Bessel beam pulses to fabricate embedded diffraction gratings in three distinct optical glasses. Although the different laser-matter interactions taking place for each material proved a challenge to produce efficient diffractive elements, this was overcome by tuning the laser processing parameters, yielding gratings that operate at various light configurations.

In particular, modification of the OG530 glass showed how one can take advantage of the nonlinear filamentation effects to engrave large volumes of material in a single laser pass, which can be key to achieve a high-throughput in an industrial environment. Meanwhile, the Eagle2000 borosilicate stood out for closely reproducing the intensity distribution of the Bessel beam in the buried inscribed tracks. This enables the generation of user-defined refractive index profiles in the material by tuning the electric field distribution of the beam along its propagation direction. Lastly, bulk processing of fused silica at low periods resulted in the appearance of shielding effects which, to the best of our knowledge, had not been reported before. This produced a decrease in the length of the inscribed tracks. In spite of this, we were able to produce optical elements controlled by the state of input polarization within this material, which are of interest in the field of optical switches.

These findings therefore reinforce the value of Bessel beams as a robust tool to explore the applications of optical buried devices in both known and novel transparent materials.

CRediT authorship contribution statement

Jorge Fantova: Conceptualization, Formal analysis, Investigation, Methodology, Validation, Visualization, Writing – original draft. **Ainara Rodríguez:** Conceptualization, Formal analysis, Funding acquisition, Supervision, Writing – review & editing. **Jesús del Hoyo:** Methodology, Writing – review & editing. **Gemma G. Mandayo:** Formal analysis, Funding acquisition, Writing – review & editing. **Santiago M. Olaizola:** Conceptualization, Formal analysis, Funding acquisition, Project administration, Supervision.

Declaration of competing interest

The authors declare that they have no known competing financial interests or personal relationships that could have appeared to influence the work reported in this paper.

Data availability

Data will be made available on request.

Acknowledgments

This work has been supported by the Ministerio de Ciencia e Innovación (Spain) and the European Union: Retos Colaboración 2019, grant Teluro-AEI (RTC2019-007113-3); and Retos Colaboración 2021, grant BIOFOT (CPP2021-009001).

Beam imaging automatization software was developed by Luis Omeñaca, from CEIT-Basque Research and Technology Alliance (BRTA).

References

[1] J.A. Arns, W.S. Colburn, S.C. Barden, Volume phase gratings for spectroscopy, ultrafast laser compressors, and wavelength division multiplexing, in: R.E. Fischer, W.J. Smith (Eds.), Current Developments in Optical Design and Optical Engineering VIII, Vol. 3779, International Society for Optics and Photonics, SPIE, 1999, pp. 313–323.

[2] P. Mitchell, G. Brown, R. Thomson, N. Psaila, A. Kar, 57 Channel (19× 3) spatial multiplexer fabricated using direct laser inscription, in: OFC 2014, IEEE, 2014, pp. 1–3.

[3] S.C. Barden, J.A. Arns, W.S. Colburn, Volume-phase holographic gratings and their potential for astronomical applications, in: S. D'Odorico (Ed.), Optical Astronomical Instrumentation, Vol. 3355, International Society for Optics and Photonics, SPIE, 1998, pp. 866–876.

[4] A.L. Glebov, O. Mokhun, A. Rapaport, S. Vergnole, V. Smirnov, L.B. Glebov, Volume bragg gratings as ultra-narrow and multiband optical filters, in: H. Thienpont, J. Mohr, H. Zappe, H. Nakajima (Eds.), Micro-Optics 2012, Vol. 8428, International Society for Optics and Photonics, SPIE, 2012, 84280C.

[5] J.-K. Rhee, T.S. Sosnowski, T.B. Norris, J.A. Arns, W.S. Colburn, Chirped-pulse amplification of 85-fs pulses at 250 khz with third-order dispersion compensation by use of holographic transmission gratings, Opt. Lett. 19 (19) (1994) 1550–1552.

[6] N. Bonod, J. Neauport, Diffraction gratings: from principles to applications in high-intensity lasers, Adv. Opt. Photon. 8 (1) (2016) 156–199.

[7] T.S. Chonis, A. Frantz, G.J. Hill, J.C. Clemens, H. Lee, S.E. Tuttle, J.J. Adams, J.L. Marshall, D.L. DePoy, T. Prochaska, Mass production of volume phase holographic gratings for the virUS spectrograph array, in: R. Navarro, C.R. Cunningham, A.A. Barto (Eds.), Advances in Optical and Mechanical Technologies for Telescopes and Instrumentation, Vol. 9151, International Society for Optics and Photonics, SPIE, 2014, 91511J.

[8] K. Itoh, W. Watanabe, S. Nolte, C.B. Schaffer, Ultrafast processes for bulk modification of transparent materials, MRS Bull. 31 (8) (2006) 620–625.

[9] R. Martínez-Vazquez, R. Osellame, G. Cerullo, R. Ramponi, O. Svelto, Fabrication of photonic devices in nanostructured glasses by femtosecond laser pulses, Opt. Express 15 (20) (2007) 12628–12635.

[10] Y. Shimotsuma, P.G. Kazansky, J. Qiu, K. Hirao, Self-organized nanogratings in glass irradiated by ultrashort light pulses, Phys. Rev. Lett. 91 (2003) 247405.

[11] T.T. Fernandez, S. Gross, A. Arriola, K. Privat, M.J. Withford, Revisiting ultrafast laser inscribed waveguide formation in commercial alkali-free borosilicate glasses, Opt. Express 28 (7) (2020) 10153–10164.

[12] J. del Hoyo, R.M. Vazquez, B. Sotillo, T.T. Fernandez, J. Siegel, P. Fernández, R. Osellame, J. Solis, Control of waveguide properties by tuning femtosecond laser induced compositional changes, Appl. Phys. Lett. 105 (13) (2014) 131101.

[13] A. Couairon, A. Mysyrowicz, Femtosecond filamentation in transparent media, Phys. Rep. 441 (2) (2007) 47–189.

[14] D.M. Krol, Femtosecond laser modification of glass, J. Non-Cryst. Solids 354 (2–9) (2008) 416–424.

[15] K.M. Davis, K. Miura, N. Sugimoto, K. Hirao, Writing waveguides in glass with a femtosecond laser, Opt. Lett. 21 (21) (1996) 1729–1731.

[16] E.N. Glezer, M. Milosavljevic, L. Huang, R.J. Finlay, T.-H. Her, J.P. Callan, E. Mazur, Three-dimensional optical storage inside transparent materials, Opt. Lett. 21 (24) (1996) 2023–2025.

[17] E. Bricchi, B.G. Klappauf, P.G. Kazansky, Form birefringence and negative index change created by femtosecond direct writing in transparent materials, Opt. Lett. 29 (1) (2004) 119–121.

[18] T.K. Gaylord, M.G. Moharam, Planar dielectric grating diffraction theories, Appl. Phys. B 28 (1982) 1–14.

[19] S.M. Eaton, H. Zhang, M.L. Ng, J. Li, W.-J. Chen, S. Ho, P.R. Herman, Transition from thermal diffusion to heat accumulation in high repetition rate femtosecond laser writing of buried optical waveguides, Opt. Express 16 (13) (2008) 9443–9458.

[20] L. Shah, A.Y. Arai, S.M. Eaton, P.R. Herman, Waveguide writing in fused silica with a femtosecond fiber laser at 522 nm and 1 MHz repetition rate, Opt. Express 13 (6) (2005) 1999–2006.

[21] J. Hernandez-Rueda, J. Clarijs, D. van Oosten, D.M. Krol, The influence of femtosecond laser wavelength on waveguide fabrication inside fused silica, Appl. Phys. Lett. 110 (16) (2017) 161109.

[22] S.M. Eaton, H. Zhang, P.R. Herman, F. Yoshino, L. Shah, J. Bovatsek, A.Y. Arai, Heat accumulation effects in femtosecond laser-written waveguides with variable repetition rate, Opt. Express 13 (12) (2005) 4708–4716.

[23] P.G. Boj, J. Crespo, J.A. Quintana, Broadband reflection holograms in dichromated gelatin, Appl. Opt. 31 (17) (1992) 3302–3305.

[24] D. Meyerhofer, Dichromated gelatin, in: H.M. Smith (Ed.), Holographic Recording Materials. Topics in Applied Physics, Vol. 20, Springer Berlin Heidelberg, 1977, pp. 75–99.

[25] M.L. Ng, D. Chanda, P.R. Herman, Coherent stitching of light in multilayered diffractive optical elements, Opt. Express 20 (21) (2012) 23960–23970.

[26] J.J. Azkona, M. Gómez-Aranzadi, A. Rodriguez, T. Morlanes, J.L. de la Peña, S.M. Olaizola, Femtosecond laser fabrication of monolithic double volume phase-gratings in glass, Opt. Express 28 (20) (2020) 29054–29063.

[27] V. Stankevič, J. Karosas, G. Račiukaitis, P. Gečys, Investigation of the modifications properties in fused silica by the deep-focused femtosecond pulses, Opt. Express 31 (3) (2023) 4482–4496.

[28] P. Boucher, J.D. Hoyo, C. Billet, O. Pinel, G. Labroille, F. Courvoisier, Generation of high conical angle Bessel-Gauss beams with reflective axicons, Appl. Opt. 57 (23) (2018) 6725–6728.

[29] C. Vetter, R. Steinkopf, K. Bergner, M. Ornigotti, S. Nolte, H. Gross, A. Szameit, Realization of free-space long-distance self-healing Bessel beams, Laser Photonics Rev. 13 (10) (2019) 1900103.

[30] J. Harb, L. Talbot, Y. Petit, M. Bernier, L. Canioni, Demonstration of type a volume bragg gratings inscribed with a femtosecond Gaussian–Bessel laser beam, Opt. Express 31 (10) (2023) 15736–15746.

[31] M. Mikutis, T. Kudrius, G. Šlekys, D. Paipulas, S. Juodkazis, High 90% efficiency bragg gratings formed in fused silica by femtosecond Gauss–Bessel laser beams, Opt. Mater. Express 3 (11) (2013) 1862–1871.

[32] G. Zhang, G. Cheng, M.K. Bhuyan, C. D'amico, Y. Wang, R. Stoian, Ultrashort Bessel beam photoinscription of bragg grating waveguides and their application as temperature sensors, Photonics Res. 7 (7) (2019) 806–814.

[33] Z. Yao, X. Li, Z. Wang, Z. Xu, A. Wang, L. Huang, J. Lu, H. Wang, High-efficiency fabrication of computer-generated holograms in silica glass using a femtosecond Bessel beam, Opt. Laser Technol. 135 (2021) 106729.

[34] W. Watanabe, Y. Matushiro, K. Hatanaka, S. Juodkazis, Regeneration of a grating in PMMA inscribed by femtosecond laser Bessel beam, J. Laser Micro Nanoeng. 12 (2) (2017) 102.

[35] F. Xin, M. Flammini, F. Di Mei, L. Falsi, D. Pierangeli, A.J. Agranat, E. DelRe, Using Bessel beams to induce optical waveguides, Phys. Rev. A 11 (2) (2019) 024011.

[36] S.M. Eaton, M.L. Ng, R. Osellame, P.R. Herman, High refractive index contrast in fused silica waveguides by tightly focused, high-repetition rate femtosecond laser, J. Non-Cryst. Solids 357 (11) (2011) 2387–2391, 17th International Symposium on Non-Oxide and New Optical Glasses (XVII ISNOG).

[37] H. Zhang, S.M. Eaton, J. Li, A.H. Nejadmalayeri, P.R. Herman, Type II high-strength bragg grating waveguides photowritten with ultrashort laser pulses, Opt. Express 15 (7) (2007) 4182–4191.

[38] K.S. Bindra, S.M. Oak, K.C. Rustagi, Optical limiting in semiconductor-doped glasses, Opt. Commun. 124 (5) (1996) 452–456.

[39] F.R. Henrique, Optical Nonlinearities in Microstructures Produced by Ultrashort Laser Pulses (Ph.D. thesis), Instituto de Física de São Carlos - Universidade de São Paulo, 2021.

[40] P. Kabaciński, T.M. Kardaś, Y. Stepanenko, C. Radzewicz, Nonlinear refractive index measurement by SPM-induced phase regression, Opt. Express 27 (8) (2019) 11018–11028.

[41] P. Polesana, M. Franco, A. Couairon, D. Faccio, P. Di Trapani, Filamentation in Kerr media from pulsed Bessel beams, Phys. Rev. A 77 (2008) 043814.

[42] D. Tan, X. Sun, J. Qiu, Femtosecond laser writing low-loss waveguides in silica glass: highly symmetrical mode field and mechanism of refractive index change, Opt. Mater. Express 11 (3) (2021) 848–857.

[43] P. Wu, C. Sui, W. Huang, Theoretical analysis of a Quasi–Bessel beam for laser ablation, Photonics Res. 2 (3) (2014) 82–86.

[44] J. Dudutis, P. GeČys, G. RaČiukaitis, Non-ideal axicon-generated Bessel beam application for intra-volume glass modification, Opt. Express 24 (25) (2016) 28433–28443.

[45] M. Osbild, E.-A. Gerhorst, S. Sivankutty, G. Pallier, G. Labroille, Submicrometer surface structuring with a Bessel beam generated by a reflective axicon, J. Laser Appl. 33 (4) (2021) 042013.

[46] D. McGloin, K. Dholakia, Bessel beams: diffraction in a new light, Contemp. Phys. 46 (1) (2005) 15–28.

[47] N. Mphuthi, R. Botha, A. Forbes, Are Bessel beams resilient to aberrations and turbulence? J. Opt. Soc. Amer. A 35 (6) (2018) 1021–1027.

[48] Q. Sun, T. Lee, M. Beresna, G. Brambilla, Control of laser induced cumulative stress for efficient processing of fused silica, Sci. Rep. 10 (3819) (2020).

[49] M.G. Moharam, L. Young, Criterion for Bragg and Raman–Nath diffraction regimes, Appl. Opt. 17 (11) (1978) 1757–1759.

[50] H. Kogelnik, Coupled wave theory for thick hologram gratings, Bell Syst. Tech. J. 48 (9) (1969) 2909–2947.

[51] A. Dias, A. Rodríguez, M. Martínez-Calderón, M. Gómez-Aranzadi, S.M. Olaizola, Ultrafast laser inscription of volume phase gratings with low refractive index modulation and self-images of high visibility, Opt. Express 23 (20) (2015) 26683–26688.

[52] A.Y. Meshalkin, V.V. Podlipnov, A.V. Ustinov, E.A. Achimova, Analysis of diffraction efficiency of phase gratings in dependence of duty cycle and depth, J. Phys. Conf. Ser. 1368 (2) (2019) 022047.

[53] M. Beresna, M. Gecevičius, P.G. Kazansky, Polarization sensitive elements fabricated by femtosecond laser nanostructuring of glass[invited], Opt. Mater. Express 1 (4) (2011) 783–795.